12-2003

Development and Validation of a 3-D Model to Predict Knee Joint Loading During Dynamic Movement

Scott G. McLean
Cleveland Clinic Foundation, mcleans@bme.ri.ccf.org

Anne Su
Cleveland Clinic Foundation

Antonie J. van den Bogert
Cleveland State University, a.vandenbogert@csuohio.edu

Original Citation

McLean, S. G., Su, A., and van den Bogert, A. J., 2004, "Development and Validation of a 3-D Model to Predict Knee Joint Loading during Dynamic Movement," Journal of Biomechanical Engineering, 125(6) pp. 864-874.

Development and Validation of a 3-D Model to Predict Knee Joint Loading During Dynamic Movement

S. G. McLean[1]

A. Su

A. J. van den Bogert

Department of Biomedical Engineering,
The Cleveland Clinic Foundation,
Cleveland, OH

The purpose of this study was to develop a subject-specific 3-D model of the lower extremity to predict neuromuscular control effects on 3-D knee joint loading during movements that can potentially cause injury to the anterior cruciate ligament (ACL) in the knee. The simulation consisted of a forward dynamic 3-D musculoskeletal model of the lower extremity, scaled to represent a specific subject. Inputs of the model were the initial position and velocity of the skeletal elements, and the muscle stimulation patterns. Outputs of the model were movement and ground reaction forces, as well as resultant 3-D forces and moments acting across the knee joint. An optimization method was established to find muscle stimulation patterns that best reproduced the subject's movement and ground reaction forces during a sidestepping task. The optimized model produced movements and forces that were generally within one standard deviation of the measured subject data. Resultant knee joint loading variables extracted from the optimized model were comparable to those reported in the literature. The ability of the model to successfully predict the subject's response to altered initial conditions was quantified and found acceptable for use of the model to investigate the effect of altered neuromuscular control on knee joint loading during sidestepping. Monte Carlo simulations (N=100,000) using randomly perturbed initial kinematic conditions, based on the subject's variability, resulted in peak anterior force, valgus torque and internal torque values of 378 N, 94 Nm and 71 Nm, respectively, large enough to cause ACL rupture. We conclude that the procedures described in this paper were successful in creating valid simulations of normal movement, and in simulating injuries that are caused by perturbed neuromuscular control.

Introduction

The knee joint is the largest and most complex joint in the human body. Comprised of multiple structures, including ligaments, menisci and the patella, it is a major load-bearing joint. In a number of sports activities, the knee is subjected to complex 3-D loading patterns that can cause injury to the internal joint structures. Anterior cruciate ligament (ACL) injury, for example, is one of the most common and potentially traumatic sports related knee injuries. Approximately 80,000 ACL injuries occur annually within the United States, with roughly 50,000 of these requiring surgical reconstruction [1–3]. Apart from the obvious acute injury effects, knee joint musculoskeletal injury often potentiates the likelihood of significant long-term debilitation. It has been shown for example, that ACL injury presents an 8–10 fold increase in the long-term incidence of osteoarthritis [4,5].

A key to understanding the potential mechanisms of knee injury is to determine the joint loading characteristics associated with an injury-causing event. In the case of the ACL, injuries are typically non-contact in nature [6–8], occurring during the landing or stance phase of ''high-risk'' sporting postures that incorporate sudden deceleration and/or rapid speed or direction changes, such as sidestepping [9,10]. It has been suggested that poor or altered neuromuscular control during these movements may produce potentially hazardous knee joint loading combinations that place the ACL at risk [3,5,8,11,12]. It is known that anterior tibial force, valgus torque and internal rotation torque all contribute to the loading of the ACL [13–15]. However, the means by which these loads may manifest during an injury causing event, and more importantly, the impact that neuromuscular control has on these loading variables, remain unclear.

Neuromuscular control during cutting/pivoting maneuvers has been quantified using kinematic, kinetic and muscle activation variables, and implications for the risk of non-contact ACL injury have been discussed [9,10,16–22]. Research of this type however, is unable to study the association between neuromuscular variables and joint loading during actual injury causing events, making the identification of ACL injury mechanisms virtually impossible.

Computer modeling and simulation techniques have been widely used to investigate injuries resulting from passive dynamic movements such as in vehicle accidents and falls [23]. Application of these techniques to actively controlled dynamic movements has recently been demonstrated in relation to overuse injuries during running activities [24,25] and ankle sprains [26]. With proper validation, models such as this offer the potential to predict the effect of neuromuscular control on knee joint loading during potentially hazardous movements such as sidestep cutting. Such models would therefore allow *in silico* experiments to study potential mechanisms of acute knee injury.

The primary purposes of this study were therefore: (1) to establish and subsequently validate a methodological approach that enabled realistic simulation of the stance phase of a sidestep cutting maneuver and subsequent estimation of the associated 3-D resultant joint loading variables: anterior-posterior force and varus-valgus and internal-external rotation torques, and (2) to demon-

[1]Department of Biomedical Engineering; The Cleveland Clinic Foundation (ND-20); 9500 Euclid Avenue; Cleveland, OH, 44195. Phone: (216)445-8857; Fax: (216)444-9198; e-mail: mcleans@bme.ri.ccf.org.

Contributed by the Bioengineering Division for publication in the JOURNAL OF BIOMECHANICAL ENGINEERING. Manuscript received by the Bioengineering Division November 16, 2003; revision received June 20, 2003. Associate Editor: C. L. Vaughan.

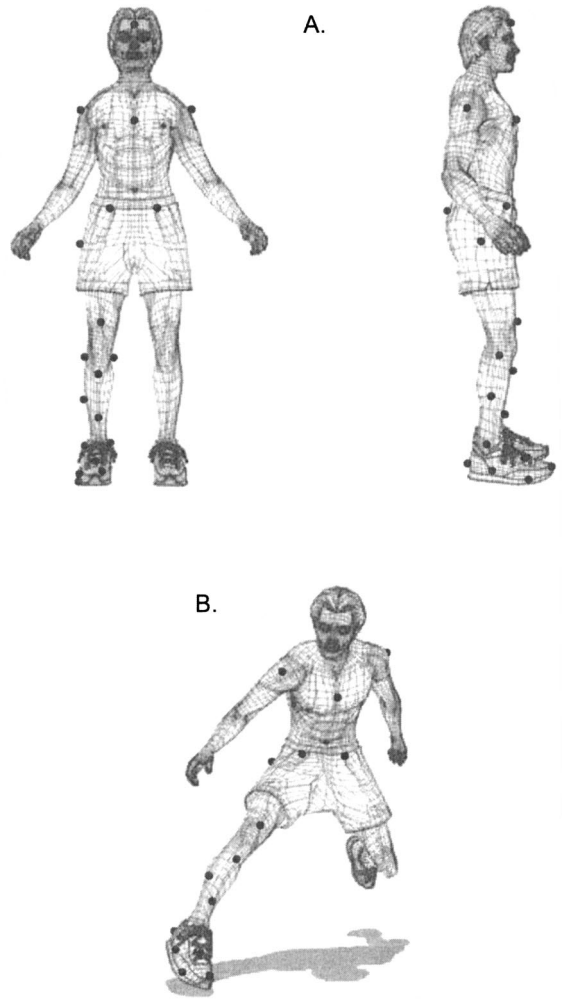

Fig. 1 Marker placements used during the collection of high speed video data. Standing (neutral) maker data (A) were used to construct a kinematic model of the trunk and lower limb. These data along with those recorded during sidestepping trials (B) were processed via Mocap Solver software to solve for the 12 degrees of freedom.

strate the utility of a model developed using this approach by predicting the effects of variability in limb posture at impact on those loads shown specifically to impact the ACL, namely, anterior force, valgus torque and internal rotation torque.

Methods

Experimental Data. Data were recorded from a single male subject (height=173 cm, weight=70 kg, age=30 years). Three-dimensional coordinates of skin-mounted markers (Fig. 1) were obtained via six electronically shuttered video cameras at 240 fps and Eva 6.0 tracking software (Motion Analysis Corp., Santa Rosa California). A standing trial was first recorded with all joints in the neutral position. The markers on the forehead, medial femoral condyle and medial and lateral malleoli were then removed prior to the recording of the motion data. The subject then performed 10 side-step cutting trials at a speed of 5.0 ± 0.3 ms^{-1}, targeting a cutting angle of 45 deg relative to the original direction of motion. Synchronized 3-D ground reaction force data were collected during each side-step trial at 1,000 Hz via an AMTI force plate (Model OR6-5, Serial #4068). By collecting data from 10 trials,

Table 1 Inertial characteristics of model representing a male subject of mass 70 kg and height 1.73 m

Segment	Mass (kg)	Length (m)	C of M pos (%)‡	Moments of Inertia (kg m^2) I^*_{xx}	I_{yy}	I_{zz}
Pelvis	5.61	0.3376	0	2.90	2.99	1.40
Femur	2.38	0.4231	40.95	0.20	0.21	0.04
Tibia	3.03	0.3526	44.59	0.03	0.03	0.005
Talus	0	0.01	0	0	0	0
Foot	0.96	0.2642	44.15	0.0047	0.0051	0.0012
Pelvis WM†	50.49	0	0	0	0	0
Thigh WM	7.53	0	0	0	0	0

‡Center of mass location was measured from the proximal to distal segment endpoints.
*I_{xx}, I_{yy} and I_{zz}=segment moment of inertia about the medio-lateral, anterior-posterior and longitudinal axes respectively.
†WM=Wobbling mass.

the movement variability of the subject (quantified as a between-trial standard deviation) will be estimated with an accuracy of about 25% [27].

From the standing neutral trial, a kinematic model comprised of five skeletal segments (foot, talus, shank and thigh of the support limb, and the pelvis) and 12 degrees-of-freedom (DOF) was defined using Mocap Solver software (version 6.14, Motion Analysis Corp., Santa Rosa, California). Mocap Solver performs model-based kinematic analysis through global least-squares optimization [28]. The pelvis was assigned 6 DOF relative to the laboratory coordinate system. The three rotational DOF (somersault, tilt, twist) were defined using the rotation sequence of Yeadon [29]. The hip joint possessed 3 DOF, with rotations (flexion-extension, abduction-adduction and internal-external rotation) defined about three orthogonal axes, passing through a fixed joint center defined according to Bell et al. [30]. Knee joint motion was described by rotation about a fixed flexion-extension axis located according to Vaughan et al. [31] and extending laterally as the subject stood in the neutral position. The ankle joint was modeled as a 2-DOF mechanism allowing rotation about talocrural and subtalar joint axes. The talocrural joint center was defined as the midpoint between the lateral and medial malleoli, with the plantar-dorsiflexion axis extending laterally from this point. This simplified orientation was justified based on known variations within a normal population [32,33]. The subtalar joint was located 10 mm directly below that of the talocrural joint [33], with its axis oriented 41° up from horizontal and 23 deg medial from the foot axis [32]. The 3-D marker trajectories recorded during the 10 side-stepping trials were processed by the Mocap Solver software to solve the 12 generalized coordinates for each frame, corresponding to the 12 DOF of the skeletal model.

Heel strike was defined as the instant when the vertical ground reaction force first exceeded 10 N. The generalized coordinate data for each trial were resampled at 1 ms intervals using linear interpolation, generating 200 resampled frames with the first frame corresponding to heel strike. The generalized speeds at heel strike were obtained using a finite difference calculation, without low-pass filtering. The generalized coordinates and speeds at heel strike were averaged over the ten trials. An ensemble average ($\pm$SD) for each rotational degree of freedom and the three ground reaction force components was also calculated across the ten trials, covering the first 200 ms of the stance phase during the side-step.

Equations of Motion. A forward dynamic 3-D rigid body model of the trunk and lower extremity was developed to represent the subject. Inertial characteristics (Table 1) were based on anthropometric data presented by de Leva [34]. The model consisted of the skeletal model described above, with wobbling masses added to the pelvis and thigh segments. Each wobbling mass segment was attached to the skeleton via a linear transla-

Table 2 Muscle properties adopted for the three-dimensional lower limb model used to simulate a sidestep

Muscle (group)	F_{max} (N)	L_{CEopt} (m)	W	PEE_{slack}	Lslack (m)	a_0	a_1	a_2	a_3	a_4	a_5	a_6
Illiopsoas	800	0.1019	1.298	1.0	0.1085	0.2304	0.03	0	0	0	0	0
Hip extensors	1300	0.1447	0.625	1.366	0.1315	0.2218	−0.076	0.015	−0.01	0	0	0
Hip adductors	1805	0.1228	0.56	1.0	0.1266	0.2310	−0.03	0.037	0.01	0	0	0
Hip abductors	1950	0.0620	0.56	1.698	0.0538	0.0693	−0.062	−0.06	0	0	0	0
Rectus femoris	780	0.0840	1.44	1.0	0.3460	0.4145	0.03	−0.03	0	0.043	0	0
Vastus lateralis	1870	0.0840	0.627	1.332	0.1570	0.2023	0	0	0	0.043	0	0
Vastus medialis	1295	0.0890	0.627	1.212	0.1260	0.1750	0	0	0	0.043	0	0
Vastus interm	1235	0.0870	0.627	1.321	0.1360	0.1834	0	0	0	0.043	0	0
Biceps femoris LH	720	0.1090	1.2	1.0	0.3410	0.4008	−0.075	0.03	0	−0.045	0	0
Biceps femoris SH	400	0.1094	1.2	1.0	0.3355	0.4116	−0.055	0.03	0	−0.04	0	0
Hamstrings	1360	0.1730	1.2	1.0	0.1000	0.2731	0	0	0	−0.045	0	0
Gastrocnemius	1605	0.0508	0.89	1.0	0.4010	0.4518	0	0	0	−0.025	−0.053	0.008
Soleus	2830	0.0300	1.039	1.616	0.2680	0.2941	0	0	0	0	−0.053	0.008
Tibialis post	1270	0.0310	0.56	1.0	0.3100	0.3496	0	0	0	0	−0.008	0.019
Tibialis ant	600	0.0980	0.442	1.0	0.2230	0.3203	0	0	0	0	0.035	0.005
Peroneals	1195	0.0516	0.56	1.0	0.2727	0.3304	0	0	0	0	−0.011	−0.021

F_{max}—Maximum isometric force
L_{Ceopt}—Optimum CE length
W—Maximum length range of force production relative to L_{CEopt}
PEE_{slack}—Slack length of PEE relative to L_{CEopt}
L_{slack}—Slack length of SEE
a_0—Muscle length in the neutral posture of the model.
a_1–a_6—Moment arms for hip flexion, hip adduction, hip internal rotation, knee extension, ankle dorsiflexion, ankle inversion-eversion respectively.

tional spring and damper with 3 DOF. The mass attached to the pelvis represented all body segments that were not modeled, including the non-support limb, arms and head. Ninety percent of the total mass of the head, arms and trunk was assigned to the wobbling mass segment with the remaining 10% being assigned to the pelvis [24]. For the thigh segment, 76% of the total mass was assigned to the soft tissue component [24]. The stiffness and damping parameters for the wobbling mass attached to the pelvis were determined via the optimization technique described later. Based on a 15 Hz natural frequency and a damping rate of 30 s^{-1} [35], the stiffness and damping parameters of the thigh wobbling mass were set to 6.4×10^4 N/m and 390 Ns/m, respectively.

A model description file for SD/FAST (Parametric Technology Corp., Needham, MA) was exported from Mocap Solver. Inertial properties and wobbling masses were added, and dynamic equations of motion were produced by SD/FAST as C code. The equations of motion are a set of second-order ordinary differential equations:

$$\mathbf{M}(\mathbf{q})\ddot{\mathbf{q}}=\mathbf{Q_M}(\mathbf{q},\dot{\mathbf{q}},\mathbf{t})+\mathbf{Q_E}(\mathbf{q},\dot{\mathbf{q}})+\mathbf{Q_C}(\mathbf{q},\dot{\mathbf{q}}) \quad (1)$$

where $\mathbf{M}$ is the mass matrix, $\mathbf{q}$ are the generalized kinematic coordinates and $\mathbf{Q_M}$, $\mathbf{Q_E}$, and $\mathbf{Q_C}$ are the generalized force terms due to, respectively, muscles, external forces, and coriolis/centrifugal forces.

Muscles. Sixteen muscles were attached to the skeleton, assuming in each a linear relationship between muscle length and the angles of the n joints that the muscle crosses:

$$L_m=a_0+a_1\phi_1+\ldots+a_n\phi_n, \quad (2)$$

where ϕ_k is the kth joint angle in radians, a_k is the moment arm of the muscle with respect to joint angle ϕ_k, and a_0 is the muscle length in the neutral posture of the model. Moment arms for all muscles (Table 2) were assumed to be constant and based on published data [36–44]. Force generation of the muscle was modeled by a three-element Hill model (Fig. 2). Muscle model equations were adapted from Van Soest and Bobbert [45] and are listed in detail in the Appendix. Muscle model parameters are listed in Table 2. Maximum isometric force in the contractile element (CE), optimal CE length and SEE slack length were taken from the work of Delp [46]. The width parameters W of the CE force-length relationships were taken from the work of Walker and Schrodt [47] and Gerritsen et al. [48]. The force F produced by each muscle (equation Appendix A) was converted into its equivalent of n joint moments using the constant moment arms defined in Eq. (2).

For each muscle, the parameter a_0 in Eq. (2) was adjusted such that maximal isometric force was generated at joint angles identified previously in literature. Specifically, maximal isometric force for the hip flexor and hip extensor muscles occurred at 30 deg and 45 deg of hip flexion respectively [49]. Maximal knee flexor and knee extensor force occurred at 5 deg knee extension and 60 deg knee flexion [50]. For the plantar flexors, maximal isometric force occurred at 15 deg dorsiflexion [51], while the dorsi flexors produced maximum force at 15 deg plantar flexion [52]. Similarly, maximum eversion force was generated at 5 deg inversion, while maximum inversion force was generated at 5 deg eversion. For hip abduction-adduction and external-internal rotation, the muscles producing these movements were assumed to generate maximum isometric force in the neutral (0 deg rotation) position.

Muscle activation dynamics were modeled as a first-order differential equation [53] to solve active state a:

$$\dot{a}(t)=(c_1u(t)+c_2)(u(t)-a(t)) \quad (3)$$

where $c_1=3.3\ s^{-1}$ and $c_2=16.7\ s^{-1}$, resulting in time constants of 50 ms and 60 ms for activation and deactivation, respectively [54]. The neural stimulation input $u(t)$ was modeled as a piecewise linear function of time, with five parameters: the stimulation

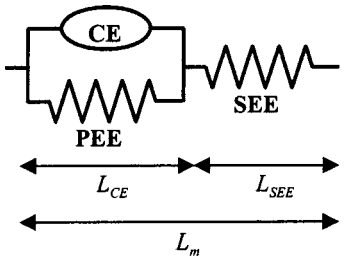

$$L_{SEE}=L_m-L_{CE}$$
$$L_{PEE}=L_{CE}$$
$$F_{CE}=F_{SEE}-F_{PEE}$$

Fig. 2 Three-component Hill model for muscle force production: contractile element (CE), parallel elastic element (PEE), and series elastic element (SEE). The corresponding relationships between lengths and forces are shown.

value at times 0, 50, 100, 150, and 200 ms after heel strike. The 16 muscles were grouped into 11 functional groups, each with a different control input $u(t)$. Neuromuscular control of the model during the movement was thus represented by 55 parameters.

Ground Contact Model. Contact between the foot and ground was modeled using 35 discrete viscoelastic elements. Each element was attached to the rigid foot segment in 3-D locations describing the exterior shoe surface. Each element permitted deformation perpendicular to the floor, representing the viscoelastic properties of the combined shoe sole and soft tissue structures and the intrinsic deformation of the foot. The vertical force-deformation relationship was modeled as:

$$F_z = k \cdot z \quad b \cdot z \cdot v_z \tag{4}$$

where z is the vertical deformation and v_z is its first derivative. The numerical values for the parameters were $k = 2500\ \mathrm{N\ m^{-1}}$ and $b = 500\ \mathrm{N\ s\ m^{-2}}$. The stiffness parameter k was chosen such that a static deformation of about 10 mm occurred under full body weight on the foot. The damping parameter b was then selected to produce force-deformation loops similar to those presented by Aerts and De Clercq [55].

Horizontal forces were modeled as an approximation of Coulomb friction.

$$F_x = \begin{cases} \mu \cdot F_z & \text{if } v_x < -\dfrac{\mu F_z}{b} \\ -b \cdot v_x & \text{if } -\dfrac{\mu F_z}{b} < v_x < \dfrac{\mu F_z}{b} \\ -\mu \cdot F_z & \text{if } v_x > \dfrac{\mu F_z}{b} \end{cases} \tag{5}$$

where b is a large positive constant (700 Ns/m). We found that the horizontal ground reaction forces rise more smoothly when the coefficient of friction μ is lower at low vertical load:

$$\mu = 1 - e^{-F_z / F_0} \tag{6}$$

where parameter F_0 had a value of 60 N. The friction coefficient saturates quickly to a value of 1.0.

Simulation and Optimization. The mean body segment positions and velocities obtained at heel strike from the experimental data were used as initial kinematic conditions for the sidestep simulation. The initial positions and velocities for the wobbling masses were chosen so that their spring attachments to the skeleton produced zero force. The rationale for this choice is that all body segments were in free fall prior to ground contact. Initial conditions for the muscle state variables a and L_{CE} were obtained by assuming steady state at heel strike, that is, setting $\dot{a}$ and $\dot{L}_{CE}$ to zero in Eqs. (3) and (*A*.7) and solving for a and L_{CE}. The equations of motion generated by SD/FAST, along with the differential equations for muscle contraction (*A*.8) and muscle activation (3) were integrated using a variable step fourth-order Runge-Kutta method.

An optimized simulation of a subject specific side-step was generated by searching for the 55 muscle control parameters and the six stiffness and damping parameters of the pelvis wobbling mass that minimized the difference between simulation and corresponding measurements. The optimization problem was defined as:

$$\text{minimize } J(\mathbf{p}) = \sum_{j=1}^{12} \sum_{i=1}^{200} \left[\frac{V_{ij} - \hat{V}_{ij}}{SD_j} \right]^2 \tag{7}$$

where

$\mathbf{p} = (p_1 \ldots p_{61})$, the vector of model parameters to be optimized

V_{ij} = measured value (mean of all trials) of variable j at time step i

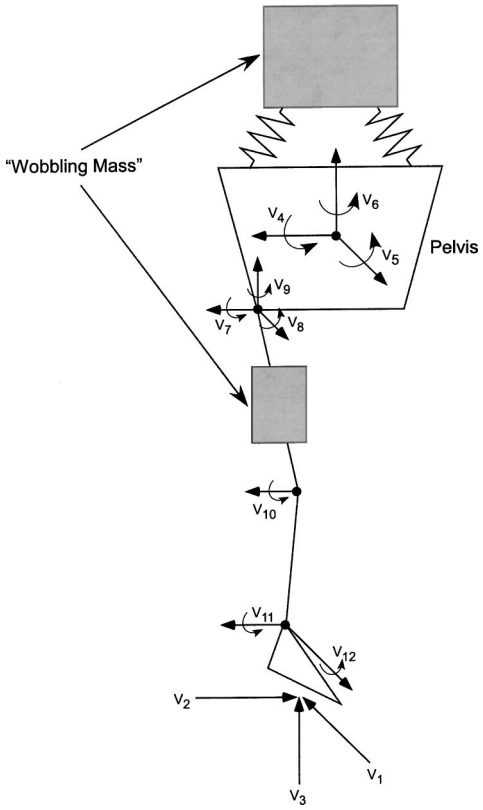

Fig. 3 Measured variables incorporated within the model optimization, comprising three ground reaction forces ($V_1 - V_3$), three body rotations ($V_4 - V_6$) and six joint rotations ($V_7 - V_{12}$).

$\hat{V}_{ij}$ = simulation result corresponding to V_{ij}

SD_j = the between-trial standard deviation in variable j, averaged over the 200 time samples

The cost function included 12 variables: three components of the ground reaction force, the three parameters describing the global orientation of the pelvis, and the rotations at the hip, knee and ankle joints (Fig. 3). The optimization problem was solved using a simulated annealing algorithm [56]. The optimization was terminated when the optimum cost function did not decrease by 1% within 1,000 simulations.

Model Validation. The first criterion for model validity was a requirement that the differences between simulation and measurements should be, on average, less than two between-trial standard deviations. Specifically, given the set of 10 normal performances of the subject, the simulated performance would be considered ''abnormal'' when more than two standard deviations from the mean. Thus from Eq. (7), the optimized model was required to produce a cost function of less than 9,600. The contributions of each of the 12 variables to the cost function were also quantified.

The second measure of model validity was its ability to predict the effect of perturbations in initial conditions. The initial (position and velocity) conditions from each trial were used as individual inputs into the optimized system, and single-trial simulations were performed. The difference between the resultant simulated and measured value for each of the movement and GRF variables was calculated at each of the 200 time-steps and a root mean square (RMS) prediction error was then quantified across the ten trials for each variable. Specifically, for a measured variable (V):

$$RMS_{ij} = \sqrt{\frac{\sum_{k=1}^{m}(V_{ijk} - \hat{V}_{ijk})^2}{m}} \quad (8)$$

where,

V_{ijk}=measurement of variable j at time i during trial k

$\hat{V}_{ijk}$=simulated data corresponding to V_{ijk}

m=number of trials

The RMS prediction errors for each variable were divided by the corresponding between-trial variability measurement (SD) from the measured data. This ratio was subsequently averaged over the 200 time samples, providing a normalized ''RMS prediction error'' value for each variable. A second RMS prediction error was also calculated, based on the first 100 samples only.

Extraction of Resultant Knee Joint Loads. For the optimized system, A-P knee joint force and varus-valgus and internal-external rotation knee moments were extracted as a function of time (0–200 ms). Data for each of these variables were obtained directly from the SD/FAST multibody software as resultant joint loads. These loads represent the externally applied ground reaction forces transmitted to the knee joint, while accounting for inertial effects of the masses in between. Based on the orientation of the knee joint coordinate system, external anterior drawer force, varus moment, and internal rotation moment were all defined as positive.

Application Example: Effect of Neuromuscular Control on Knee Joint Loading. Monte Carlo simulations (N=100,000) were performed to determine the effects of variability in neuromuscular control on peak anterior drawer force, valgus moment and internal rotation moment. Specifically, pre-impact body segment angular positions and angular and linear velocities were randomly perturbed, representing a Gaussian distribution based on measured variability for each of the movement variables across the ten sidestepping trials. Initial vertical position of the model was always set such that the lowest foot contact point was at $z=0$. Resultant loading variables (anterior force, valgus torque and internal rotation torque) were extracted for each simulated trial and peak values were subsequently determined and stored for analyses.

Results

A single simulation of the first 200 ms of stance for the sidestep required between 0.5 and 1.2 s of CPU time on a Pentium III 800 MHz processor. The optimization algorithm terminated after approximately 165,000 simulations. The cost function was minimized to a value of $J=2674$. Repeated runs of the simulated annealing algorithm, with new random number seeds, always resulted in the same solution. Comparisons between measured and simulated sidestep data for the first 200 ms of stance are presented for key kinematic and GRF variables (Fig. 4). The optimized muscle activation parameters (n=5) for the 11 functional muscle groups that produced these movements, and comparative data reported previously for a similar movement [18], are also presented (Fig. 5). The optimization identified muscle activation and wobbling mass stiffness/damping parameter values that, except in the case of body tilt, produced movement and GRF variables that were within two standard deviations of the measured subject data (Table 3, RMS fit values).

RMS prediction errors over 200 ms for the optimized system for several movement (somersault, hip flexion-extension, knee flexion-extension and ankle plantar-dorsi flexion) and GRF (anterior-posterior and medio-lateral force) variables were within two standard deviations of measured between-trial variability values (Fig. 6). For other variables however (e.g., Vertical force, tilt, twist and ankle inversion-eversion), RMS prediction errors were much larger (Table 3, RMS pred values). RMS prediction errors calculated for each variable over the first 100 ms only, were considerably smaller than the corresponding 200 ms value, except in the case of anterior-posterior and medio-lateral GRF's (Table 3).

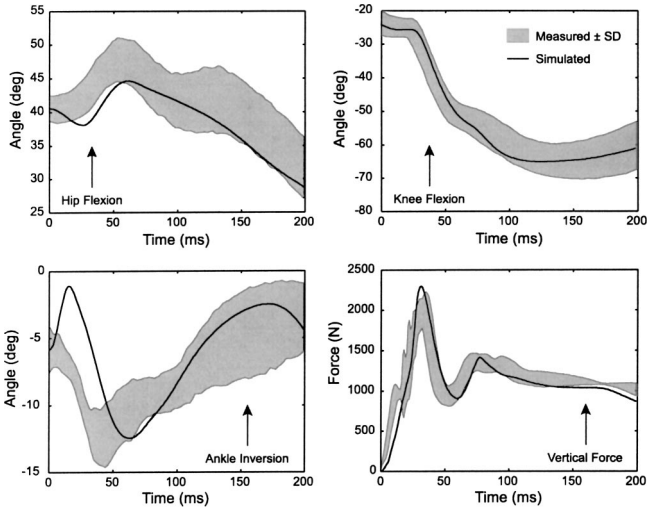

Fig. 4 Comparisons between measured and simulated sidestep data for the first 200 ms of stance for key movement (hip flexion-extension, knee flexion-extension and ankle inversion-eversion) and GRF (vertical force) variables.

The anterior-posterior resultant joint reaction force between the tibia and femur, varus-valgus and internal-external knee moments are shown in Fig. 7 for the optimized simulation. A peak anterior drawer force of 34.6 N was observed, occurring at heel strike, with a peak posterior force of 118.6 N occurring 61 ms after impact. Peak varus and valgus moments of 8.51 Nm and 19.15 Nm were observed to occur 59 ms and 10 ms after impact respectively. Peak internal and external rotation moments of 19.24 Nm and 0.74 Nm occurred 75 ms and 184 ms after impact, respectively.

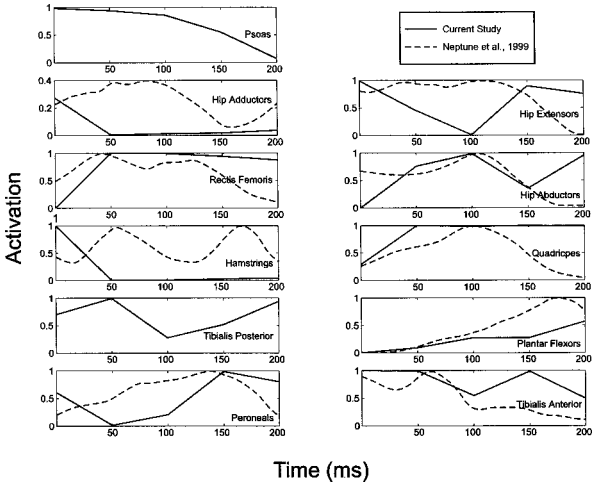

Fig. 5 Optimized muscle activations for the 11 functional muscle groups used in the simulation of the sidestep cutting maneuver. Activation patterns for each group were modeled as a 5 parameter piecewise linear functions of time. Quadriceps activations represented those applied to the vastus lateralis, medialis and intermedius muscles. Hamstring activation patterns were applied to the hamstring and biceps femoris (short and long head) muscles. Plantar flexor activations were applied to the gastrocnemius and soleus muscles. Comparisons are also made between these and similar data reported previously for sidestepping maneuvers [18].

Table 3 Validity measures for simulated model variables. RMS fit error corresponds to the average number of SD's each simulated variable is away from the corresponding measured value. RMS prediction error was represented as the ratio of the mean RMS difference between the ten subject-specific sets of measured and simulated data, to the mean measured inter-trial variability, over both 200 and 100 ms.

VARIABLE	*RMS fit/SD*	RMS pred/SD (200 ms)	RMS pred/SD (100 ms)
Medio-Lateral Force (Fx)	0.97	1.24	1.13
Anterior-Posterior Force (Fy)	0.89	1.85	2.42
Vertical Force (Fz)	1.29	3.17	1.61
Somersault (Rx)	0.55	0.98	0.59
Tilt (Ry)	2.13	9.36	3.40
Twist (Rz)	0.86	4.55	3.79
Hip Flexion-Extension (Hx)	1.01	1.31	1.06
Hip Abduction-Adduction (Hy)	0.67	2.05	1.58
Hip Axial Rotation (Hz)	0.79	2.72	1.63
Knee Flexion-Extension (Kx)	0.36	0.61	0.59
Ankle Planter-Dorsi Flexion (Ax)	0.69	1.34	0.95
Ankle Inversion-Eversion (Ay)	1.01	4.15	3.29

Random perturbations in initial body and segment positions and velocities produced noticeable increases in the resultant anterior drawer force and valgus and internal rotation knee moments (Fig. 8). Monte Carlo simulations resulted in a peak anterior drawer force, valgus and internal rotation torques as high as 377.4 N, 93.5 Nm and 70.6 Nm respectively.

Discussion

The primary objective of this study was to develop and subsequently validate a subject-specific 3-D model of the lower extremity that could simulate normal and perturbed sidestep cutting maneuvers and hence, be used to predict specific resultant knee joint loads linked to ACL injury. A forward dynamic simulation of a side-step that reproduced experimental data obtained from a single subject was generated for this purpose.

Optimization and Validation. Approximately 37 hours of computing time (165,000 simulations) were required to obtain an optimized solution to the forward dynamic problem. Neptune et al. [24] used a similar approach to obtain a dynamic simulation of running, using the DADS multibody software. Only 5,000 simulations were used to perform the optimizations, which was reported to require 660 hours of computation. With the software based on SD/FAST we therefore reached a 600-fold increase in computation speed, which allowed us to solve the optimization problem much faster as well as perform more than 30 times the number of simulations. Repeated optimizations could therefore be conducted, which resulted in identical solutions, confirming that a global optimum had probably been found.

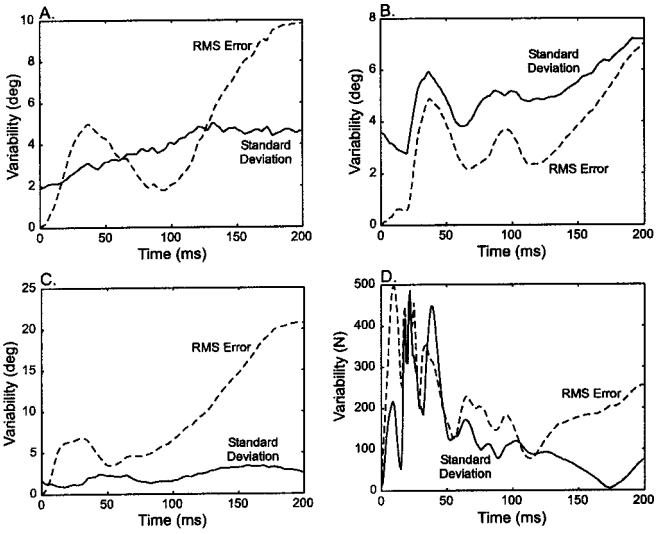

Fig. 6 Comparisons between model RMS prediction errors and measured between-trial variability over 200 ms, for key movement (A. hip flexion-extension, B. knee flexion-extension and C. ankle inversion-eversion) and GRF (D. vertical force) variables

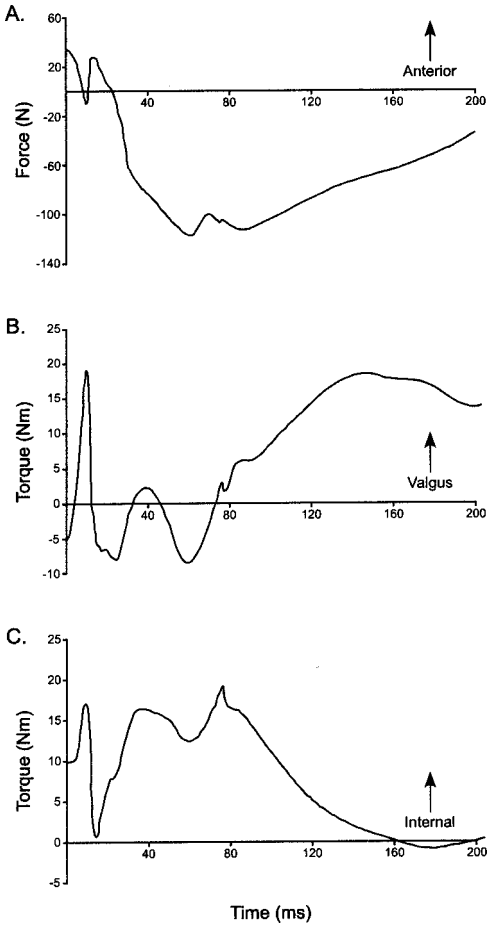

Fig. 7 External 3D knee joint reaction forces calculated for the optimized sidestep simulation. Peak anterior force (A), valgus (B) and internal rotation torque (C) values of 34.6 N, 19.15 Nm and 19.24 Nm respectively, were observed over the first 200 ms of stance

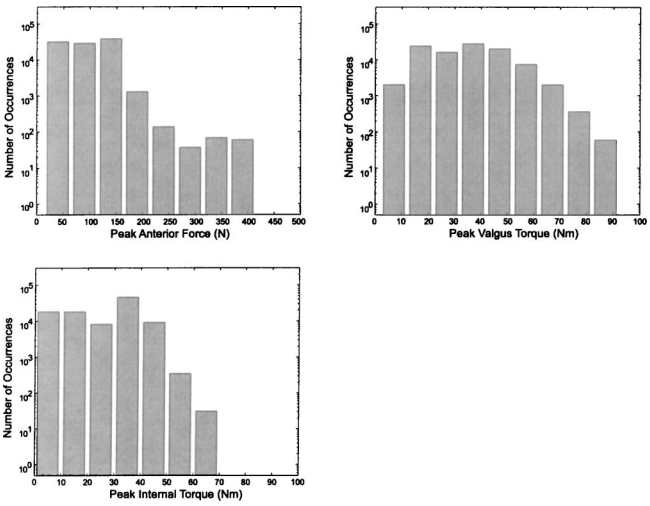

Fig. 8 Monte Carlo simulations (n=100000), representing realistic variations in neuromuscular control at impact, produced large increases in anterior knee joint reaction force, and valgus and internal rotation torques over the first 200 ms of stance during simulated sidestepping trials

The RMS fit results (Table 3) suggest that the optimized model was able to simulate a sidestep cutting maneuver that was consistent with movements performed by the subject. Except for body tilt, all simulated movements and GRF's fell within two standard deviations of the mean measured subject data over the 200 ms simulation window, with 10 of the 12 variables falling within one standard deviation. The discrepancy between mean measured and simulated data observed for body tilt may be caused by the use of a lumped upper-body model and the lack of active muscle control on the wobbling mass. Joint angle patterns and peak ground reaction force magnitudes obtained for the optimized solution were similar to those previously obtained in other experimental studies [10,17].

Previous studies [24,26] have not achieved fit errors as low as reported here. These studies modeled neural excitation patterns for each muscle as block functions defined by three parameters only, compared to piecewise linear functions of time, with five parameters in the current model. We found that optimization of block functions resulted in increased deviation from the measured data. Furthermore, the relatively long time taken previously to perform one simulation [24], limited the number of simulations that could be run in a reasonable time. It is therefore possible that a global solution to the optimization problem was not achieved previously.

Optimized activation patterns for the major muscle groups were consistent with EMG data presented previously for similar movements. Similar to our results, Colby et al. [10] found low hamstring and very high (peak at 250% MVC) quadriceps activations during the stance phase of the side-step. Quadriceps activations observed for the optimized system were also similar to those reported by Neptune et al. [18], where an increase in activation was seen following impact (Fig. 5). The activation patterns of the hip abductor, plantar flexor, peroneal and tibialis anterior muscles observed in the current study were similarly consistent with those reported by Neptune et al. [18]. Direct comparisons are difficult however, due to the lack of EMG magnitude normalization [18], or the lack of timing information and movement consistency [10] in the experimental studies.

The ability of the model to predict a response to variations in initial kinematic conditions was assessed. This aspect of the model is important for applications where the effect of neuromuscular control on knee joint loading is studied. These effects are an important component of current thinking on ACL injury mechanisms [6,7]. Wright et al. [26] developed a computer model to examine the influence of initial foot position on ankle sprains. The model's response to perturbations in the ground surface was observed to be similar to that demonstrated by the subject and it was concluded that the model could be extended for experiments that could not be performed on subjects, such as in the case of a sprain-inducing event. Our evaluation of predictive ability of the model is based on a similar concept, though with a more formal quantitative analysis. An RMS prediction error was determined for each simulated variable, averaged over the duration of the simulation, and normalized to the measured inter-trial variability. Representing predictive error in this way is a simple and intuitive means to quantify model validity. Prediction errors smaller than one standard deviation indicate that the model is useful because in that case the simulation produces a better prediction than simply using an average of previous measurements. Furthermore, we found that quantifying validity in this way was a very effective method of deciding when changes to the model were improvements. Adding more free parameters to a model will always reduce the fit error, but will not always reduce the prediction error. ''Overfitting'' the model by adding excessive complexity can thus be avoided.

Relatively large RMS prediction errors were observed for body tilt and twist, vertical ground reaction force and ankle inversion-eversion. The inability of the model to successfully predict body tilt and body twist for a given set of initial kinematic conditions may be a result of approximating the upper body as a single rigid segment. The upper body segment comprising the trunk, head, arms and the non-contact limb, possessed a large percentage of the entire mass of the system. With no active muscle control allocated to this segment, the ability of lower limb musculature to control its motion during the simulated movement is likely to be limited. Neptune et al. [24] suggested that the modeling of specific upper-body segments has the potential to improve a model's ability to reproduce lower limb movements. This appears worth consideration in future developments of the current model. The inability of the model to predict vertical GRF past 100 ms is probably also related to the lack of active control of the upper body, where most mass is located. The relatively large prediction errors observed for ankle inversion-eversion were found to result from the almost flat-footed landing in this subject, which made initial foot rotations sensitive to initial joint angles and ground contact geometry. In a second subject, who performed the movement differently, these prediction errors were found to be much smaller.

The RMS prediction errors calculated over the first 100 ms of the simulation were generally smaller than the 200 ms prediction errors (Table 3). An exponential increase of prediction error over time is to be expected from forward dynamic simulation of an unstable system using open loop muscle stimulation. Non-contact ACL injuries are reported to occur early in stance [57], and our initial results suggest that movements and GRF's during early stance are more sensitive to limb posture at impact than to the muscle activation after impact. For injuries that occur later on in the stance phase, the modeling approach described here may be less effective.

Model Limitations. Kinematic data were used as initial conditions for the simulation, and as targets for the optimization process. Error propagation analysis using Mocap Solver indicated that all measured degrees of freedom were robust against errors in marker trajectories, such as those caused by noise or skin movement. In the simulations, we noticed that results, especially the ankle rotations and ground reaction forces, were moderately sensitive to the measured initial generalized velocities $\dot{\mathbf{q}}$. It is well known that such velocity measurements are sensitive to high-frequency noise, and we considered using low-pass filtering. However, at impact the velocity of the foot decreases very quickly from about 4 m/s to zero. Low-pass filtering caused temporal blurring and led to underestimation of impact velocities. We found that simulation results were more consistent without low pass filtering, but some effect of measuring error remains inevitable.

The knee joint mechanism was modeled as a simple hinge. This neglects the posterior shift of the joint axis that is known to occur during flexion. If moment arms of muscles had been modeled using their bony attachments, this would have led to large errors in moment arms at the knee. However, we modeled the muscle path analytically (Eq. 2), which eliminates that problem. What remains is an effect on whole body dynamics and joint loading. A moving joint axis would affect whole body motion, and hence ground reaction forces and joint loading, but this effect is obviously small relative to the gross movement of body mass. The second simplification was that internal-external rotation of tibia with respect to the femur was not included in the model. This would transfer all internal-external rotation to the hip joint, effectively adding the femur mass to the rotational inertia of the tibia. A sensitivity analysis showed that this had only a minor impact on model performance. An additional consideration was that accurate measurement of internal-external knee rotation in the subject would be needed, which is almost impossible [58] and might have introduced additional error into the movement simulations. It was therefore decided not to include this degree of freedom in the model.

Muscle paths were modeled using constant moment arms (Eq. 2). It has been reported that the moment arm of the quadriceps can change as much as 50% over the 65 deg range of knee flexion that occurs during a sidestep [59]. We obtained our moment arms from an in vivo methodology [39], which did not report substantial changes in moment arms of hamstrings and quadriceps during knee flexion. A sensitivity analysis revealed that a model with either a 50% increase or decrease in the knee moment arms of the quadriceps (rectis femoris, vastus medialis, vastus lateralis and vastus intermedius) produced only small changes in the resultant knee joint loading variables after reoptimization of the muscle stimulation patterns. Specifically, peak values for resultant anterior force, valgus moment and internal rotation moment were all within 8.1%, 14.7% and 12.3% of the original baseline loads. Furthermore, these peaks occurred within ± 2 ms of those extracted from the baseline optimization. The minimum cost functions obtained for the re-optimized systems were within 2.3% of that obtained for the original optimization, suggesting that a sidestepping maneuver could still be simulated successfully within this range of quadriceps moment arm lengths. It was therefore felt that more detailed modeling of moment arms as a function of joint angle would not necessarily improve accuracy of current model outputs, nor better achieve the stated project goals.

Knee Joint Loading. As noted earlier, joint loading variables were obtained directly from the SD/FAST multibody software as resultant joint loads. These loading variables are the same as those that would be obtained using a standard inverse dynamics approach. Obtaining these data via a forward dynamic optimization approach however, rather than via an inverse analysis, allows us to predict how these resultant loads would be affected by neuromuscular control.

A resultant posterior force on the knee was observed throughout stance for the optimized sidestep model (Fig. 6). This result can be understood as follows. With the hip and knee slightly flexed at initial contact, the impact phase of the sidestep, involving rapid deceleration of the body on a planted foot, will necessarily result in posterior force being applied externally to the knee joint. It is, however, important to understand that this resultant force should not be interpreted as the force in passive joint structures. Muscle forces induce equal and opposite reaction forces in passive joint structures, and these therefore cancel out in the resultant. Our model predicted muscle forces, but did not include an accurate 3-D model of musculoskeletal geometry. Such a model would be needed to quantify muscular contributions to the resultant joint loads, and is a likely progression of the current model so that loading of the passive structures can be estimated in future studies. It has been postulated that the quadriceps force, which produces an anterior tibial load when the knee is between approximately $0°-30°$ of flexion [60,61], can produce an injury to the ACL [7,62]. When we computed contribution of the quadriceps to the anterior-posterior knee force using a 2-D model [38], we indeed found an anterior drawer force acting on the passive joint structures. However, the highest value found during the Monte Carlo simulations was only 872.4 N, while it takes at least 2,000 N to rupture the ACL [63]. We therefore conclude that this injury mechanism is unlikely to occur during sidestepping, as was also suggested by Simonsen et al. [19], and that rotational loading is required to injure the ACL.

Peak internal-external rotation moments observed during stance for the optimized side-step were similar to those reported previously. Besier et al. [64] observed a mean peak internal rotation moment of approximately 0.35 $\mathrm{Nm \cdot kg^{-1}}$ during what was termed the peak push-off phase of the sidestep, representing 10% either side of the peak vertical GRF. Little or no evidence of a net resultant external rotation moment was observed during the stance phase of the sidestep [64]. Peak internal-external moments reported for the current model, while slightly smaller, occurred during similar phases of the movement. The differences in the moment magnitudes between the two studies may be due to different cutting angles and speeds.

Besier et al. [64] also reported peak varus and valgus moments of approximately 0.35 $\mathrm{Nm \cdot kg^{-1}}$ and 0.4 $\mathrm{Nm \cdot kg^{-1}}$ respectively to occur during sidestep stance. Specifically, a net varus moment was evident during the peak-push-off phase, while valgus moments occurred during weight acceptance, representing heel-strike to the first trough in the vertical GRF and final push-off, the last 15% of the stance phase. For the current model, varus and valgus moments and the associated peaks occurred during similar phases of ground contact to those reported by Besier et al. [64]. Again, discrepancies between the two studies regarding the magnitudes of these moments may be due to differences in the protocol.

A rapid change in magnitude was observed for all three resultant loads extracted from the optimized system immediately following contact, peaking 10 ms into stance. The peaks were associated with simultaneous transients in the horizontal GRF and were found to be sensitive to the initial hip abduction-adduction velocity input into the model. As noted earlier, initial angular velocities may be unreliable because of measurement noise and the sudden changes in velocity that occur at impact. However, this sensitivity of valgus and internal rotation moments to initial hip angular speed also suggests that neuromuscular control of hip ab-adduction is a potential mechanism of ligament injury. To date however, there is no experimental data to support such a relationship between control of hip ab-adduction and resultant knee torques.

Random perturbations in the initial body and segment positions and velocities, representing variations in neuromuscular control, produced considerable increases in peak anterior, valgus and internal rotation loads. It is especially noteworthy that the statistical distribution of predicted peak valgus moments was much broader than that of the other variables (Fig. 8), indicating that this variable is more sensitive to initial limb posture. These data suggest that excessive valgus loading may be an important mechanism for injury during sidestepping. Piziali et al. [65] reported that ligament damage occurred in cadaveric knee joints within $125-210$ Nm of valgus torque or $35-80$ Nm of internal rotation torque. The maximum peak valgus and internal moments generated via the Monte Carlo simulations were somewhat below this range. However, in the Piziali [65] study, valgus and internal rotation torques were applied in isolation only. Both Kanamori et al. [14] and Markolf et al. [15] have demonstrated that the greatest increase in ACL loading occurs when these loads are applied in combination, and also when combined with anterior drawer. Hence, the magnitudes of the valgus and internal rotation torques generated during the MC simulations may have been large enough to produce an injury when combined. However, the influence of combined knee loading states on ACL load is only known for extremely low

levels of loading [14,15], which are not representative of the dynamic joint loads associated with sporting maneuvers such as sidestepping. Further research is required in this area so that our results can be better interpreted in terms of ACL injury.

Summary and Conclusions

A subject-specific 3-D rigid body model of the trunk and lower extremity, capable of simulating the stance phase (0–200 ms) of a sidestep cutting maneuver, was developed and used to predict the effect of limb posture at impact on the 3-D loading of the knee joint. Our conclusions are:

1. The modeling approach was computationally feasible, with about 30 hours each required for model optimization and Monte Carlo simulations.
2. The model could be optimized to produce movements and ground reaction forces that were consistent with the subject data.
3. Predicted responses to small neuromuscular perturbations were valid for the first 100 ms of stance.
4. Monte Carlo simulations resulted in a number of simulations where knee joint loading, especially the valgus moment, approached values that may cause injury.
5. Further research is needed to study how ACL loading depends on high-level combined loading states of the knee joint.

Acknowledgments

This work was supported by a grant from the National Institutes of Health (AR47039).

Nomenclature

A = shape parameter of the CE force-velocity relationship
ACL = anterior cruciate ligament
CE = contractile element
J = cost function for optimization
M = mass matrix
PEE = parallel elastic element
SEE = series elastic element
W = dimensionless width of the CE force-length relationship
$a(t)$ = muscle active state at time t
b = damping parameter
c_1, c_2 = rate parameters for muscle activation dynamics
$\mathbf{f}$ = generalized forces
f = normalized force-length relationship of the CE
g = normalized force-velocity relationship of the CE
k = stiffness parameter
$\mathbf{q}$ = generalized kinematic coordinates
p = model parameters to be optimized
$u(t)$ = neural muscle stimulation input at time t
z = vertical deformation of a contact element attached to the foot
μ = coefficient of friction
$\lambda(a)$ = scaling factor for CE shortening velocity as a function of muscle active state
F_{CE} = force produced in the contractile element
F_0 = parameter for the change in friction coefficient as a function of compressive load
$F_{\max}$ = maximal isometric force of the CE
F_z = vertical ground reaction force
L_{CE} = length of the contractile element
L_{CEopt} = length of the CE at which maximal force can be produced
V_{CE} = lengthening velocity of the CE($=dL_{CE}/dt$)
V_{ij} = measured value (mean of all trials) of variable j at time step i
$\hat{V}_{ij}$ = simulation result corresponding to V_{ij}
V_{ijk} = measurement of variable j at time i during trial k
$\hat{V}_{ijk}$ = simulation data corresponding to V_{ijk}
a_k = moment arm of the muscle with respect to joint angle k
a_0 = muscle length in the neutral posture of the model
$g_{\max}$ = asymptotic value of g for large lengthening velocities
v_z = the first derivative of z
ϕ_k = the kth joint angle in radians

Appendix: Model for Muscle-Tendon Dynamics

Each muscle-tendon unit in the model was modeled as a three-component Hill model (Fig. 2). The contractile element (CE) was assumed to produce a force F_{CE} which depends on CE length L_{CE}, CE lengthening velocity V_{CE}, and on active state a, according to the following relationship:

$$F_{CE}=f(L_{CE})\cdot g(V_{CE},a)\cdot \max\begin{Bmatrix} a_{\min} \\ a \end{Bmatrix} \tag{A.1}$$

The minimum activation level, $a_{\min}=0.01$, was set to prevent division by zero when solving for V_{CE}. The force-length relationship f of the CE was modeled as:

$$f(L_{CE})=\max\begin{Bmatrix} F_{\min} \\ F_{\max}\ 1-\dfrac{(L_{CE}-L_{CEopt})^2}{W^2L_{CEopt}^2} \end{Bmatrix} \tag{A.2}$$

where $F_{\max}$ is the maximal isometric force, L_{CEopt} is the length of the CE at which maximal force can be produced, and W is a dimensionless parameter describing the width of the force-length relationship. A minimum force level $F_{\min}$ was needed to prevent division by zero when solving for V_{CE} in equation (A.1) and was set at 10 N.

The normalized force-velocity relationship of the CE was assumed to be independent of L_{CE} [66,67]:

$$g(V_{CE})=\begin{cases} \dfrac{\lambda(a)V_{\max}\quad V_{CE}}{\lambda(a)V_{\max}-V_{CE}/A} \\ \quad \text{if } V_{CE}\leqslant 0 \ \text{ (shortening)} \\ \dfrac{g_{\max}V_{CE}\quad d_1}{V_{CE}\quad d_1} \\ \quad \text{if } 0<V_{CE}\leqslant \gamma d_1 \ \text{ (slow lengthening)} \\ d_3\quad d_2V_{CE} \\ \quad \text{if } V_{CE}>\gamma d_1 \ \text{ (fast lengthening)} \end{cases} \tag{A.3}$$

where

$$d_1=\frac{V_{\max}A(g_{\max}-1)}{S(A\quad 1)}$$

$$d_2=\frac{S(A\quad 1)}{V_{\max}A(\gamma\quad 1)^2}$$

$$d_3=\frac{(g_{\max}-1)\gamma^2}{(\gamma\quad 1)^2}\quad 1$$

For shortening, this model is classical Hill equation [68]. The shape parameter A was assumed to have a value of 0.25, and the maximal shortening velocity $V_{\max}$ was assumed to have a value of $10\cdot L_{CEopt}$ per second [69]. A scaling factor λ was introduced to account for the influence of a voluntary activation level a on the force-velocity relationship:

$$\lambda(a)=1-e^{-3.82a}\quad a\cdot e^{-3.82} \tag{A.4}$$

This relationship fits the experimental data of Chow and Darling [70]. For slow lengthening, a second hyperbolic relationship was used. The parameter $g_{\max}$, the asymptotic value of g, was assumed to be 1.5 and the parameter S was set to a value of 2.0 to produce a doubling of slope of the force-velocity curve at zero velocity [45,71]. At high lengthening velocities, a linear force-velocity re-

lationship was assumed to ensure that g is invertible. The transition point between the hyperbolic and linear parts was defined by a dimensionless parameter γ, which should be large to approximate correct yielding behavior at high force [71]. A value of $\gamma=5.67$ was used. The constants c_2 and c_3 were defined using continuity of the curve and its first derivative.

The series elastic element (SEE) and parallel elastic element (PEE) were assumed to be nonlinear elastic, with a quadratic relationship between force F and length L:

$$F=\begin{cases} 0 & \text{if } L \quad L_{\text{slack}} \\ k(L-L_{\text{slack}})^2 & \text{if } L>L_{\text{slack}} \end{cases} \tag{A.5}$$

The stiffness parameter k for the SEE was chosen for each muscle such that the SEE elongation was 4% when the maximal isometric force of the muscle was applied [72]. The stiffness parameter of the PEE in each muscle was chosen such that the PEE force was equal to the maximal isometric force when the CE was stretched to its maximal length for active force production:

$$k_{PEE}=\frac{F_{\max}}{(W\cdot L_{CEopt})^2} \tag{A.6}$$

The slack length of the PEE was set equal to L_{CEopt}, except where indicated otherwise in Table 2.

When CE velocity is solved from Eq. (*A*.1), we obtain an ordinary differential equation (ODE) with L_{CE} as the state variable and active state a and muscle-tendon length L_m as inputs:

$$\frac{dL_{CE}}{dt}=g^{-1}\ \frac{F_{CE}}{a\cdot f(L_{CE})}\ =g^{-1}\ \frac{F_{SEE}(L_m-L_{CE})-F_{PEE}(L_{CE})}{a\cdot f(L_{CE})} \tag{A.7}$$

Finally, muscle force is computed from the state variable:

$$F_m=F_{SEE}(L_m-L_{CE}) \tag{A.8}$$

References

[1] Daniel, D. M., and Fritschy, D., 1994, Anterior Cruciate Ligament Injuries, Philadelphia, W.B. Saunders.

[2] Frank, C. B., and Jackson, D. W., 1997, ''The Science of Reconstruction of the Anterior Cruciate Ligament,'' J. Bone Jt. Surg., Am. Vol., **79**(10), pp. 1556–1576.

[3] Griffin, L. Y., Agel, J., Albohm, M. J., Arendt, E. A., Dick, R. W., Garrett, W. E., Garrick, J. G., Hewett, T. E., Huston, L., Ireland, M. L., Johnson, R. J., Kibler, W. B., Lephart, S., Lewis, J. L., Lindenfeld, T. N., Mandelbaum, B. R., Marchak, P., Teitz, C. C., and Wojtys, E. M., 2000, ''Noncontact Anterior Cruciate Ligament Injuries: Risk Factors and Prevention Strategies,'' J. Am. Acad. Orthop. Surg., **8**(3), pp. 141–150.

[4] Gilquist, J., and Messner, K., 1999, ''Anterior Cruciate Ligament Reconstruction and the Long-Term Incidence of Gonarthrosis,'' Sports Med., **27**(3), pp. 143–156.

[5] Sutton, A. J., Muir, K. R., Mockett, S., and Fentem, P., 2001, ''A Case-Control Study to Investigate the Relation Between Low and Moderate Levels of Physical Activity and Osteoarthritis of the Knee Using Data Collected as Part of the Allied Dunbar National Fitness Survey,'' Ann. Rheum. Dis., **60**, pp. 756–764.

[6] Boden, B. P., Dean, G. S., Feagin, Jr., J. A., and Garrett, Jr., W. E., 2000, ''Mechanisms of Anterior Cruciate Ligament Injury,'' Orthopedics, **23**(6), pp. 573–578.

[7] Feagin, Jr., J. A., and Lambert, K. L., 1985, ''Mechanism of Injury and Pathology of Anterior Cruciate Ligament Injuries,'' Orthop. Clin. North Am., **16**(1), pp. 41–45.

[8] Kirkendall, D. T., and Garrett, Jr., W. E., 2000, ''The Anterior Cruciate Ligament Enigma. Injury Mechanisms and Prevention,'' Clin. Orthop., (372), pp. 64–68.

[9] Cross, M. J., Gibbs, N. J., and Bryant, G. J., 1989, ''An Analysis of the Sidestep Cutting Manoeuvre,'' Am. J. Sports Med., **17**(3), pp. 363–366.

[10] Colby, S., Francisco, A., Yu, B., Kirkendall, D., Finch, M., and Garrett, Jr., W., 2000, ''Electromyographic and Kinematic Analysis of Cutting Maneuvers. Implications for Anterior Cruciate Ligament Injury,'' Am. J. Sports Med., **28**(2), pp. 234–240.

[11] McNair, P. J., Marshall, R. N., and Matheson, J. A., 1990, ''Important Features Associated With Acute Anterior Cruciate Ligament Injury,'' N. Z. Med. J., **103**(901), pp. 537–539.

[12] McLean, S. G., Myers, P. T., Neal, R. J., and Walters, M. R., 1998, ''A Quantitative Analysis of Knee Joint Kinematics During the Sidestep Cutting Maneuver. Implications for Non-Contact Anterior Cruciate Ligament Injury,'' Bull. Hosp. Jt. Dis., **57**(1), pp. 30–38.

[13] Butler, D. L., Guan, Y., Kay, M. D., Cummings, J. F., Feder, S. M., and Levy, M. S., 1992, ''Location-Dependent Variations in the Material Properties of the Anterior Cruciate Ligament,'' J. Biomech., **25**(5), pp. 511–518.

[14] Kanamori, A., Woo, S. L., Ma, C. B., Zeminski, J., Rudy, T. W., Li, G., and Livesay, G. A., 2000, ''The Forces in the Anterior Cruciate Ligament and Knee Kinematics During a Simulated Pivot Shift Test: A Human Cadaveric Study Using Robotic Technology,'' Arthroscopy, **16**(6), pp. 633–639.

[15] Markolf, K. L., Burchfield, D. M., Shapiro, M. M., Shepard, M. F., Finerman, G. A., and Slauterbeck, J. L., 1995, ''Combined Knee Loading States That Generate High Anterior Cruciate Ligament Forces,'' J. Orthop. Res., **13**(6), pp. 930–935.

[16] Arendt, E., and Dick, R., 1995, ''Knee Injury Patterns Among Men and Women in Collegiate Basketball and Soccer. NCAA Data and Review of Literature,'' Am. J. Sports Med., **23**(6), pp. 694–701.

[17] McLean, S. G., Neal, R. J., Myers, P. T., and Walters, M. R., 1999, ''Knee Joint Kinematics During the Sidestep Cutting Maneuver: Potential for Injury in Women,'' Med. Sci. Sports Exercise, **31**(7), pp. 959–968.

[18] Neptune, R. R., Wright, I. C., and van den Bogert, A. J., 1999, ''Muscle Coordination and Function During Cutting Movements,'' Med. Sci. Sports Exercise, **31**(2), pp. 294–302.

[19] Simonsen, E. B., Magnusson, S. P., Bencke, J., Naesborg, H., Havkrog, M., Ebstrup, J. F., and Sorensen, H., 2000, ''Can the Hamstring Muscles Protect the Anterior Cruciate Ligament During a Side-Cutting Maneuver?,'' Scand. J. Med. Sci. Sports, **10**(2), pp. 78–84.

[20] Yu, B., Kirkendall, D. T., Taft, T. N., and Garrett, Jr., W. E., 2002, ''Lower Extremity Motor Control-Related and Other Risk Factors for Noncontact Anterior Cruciate Ligament Injuries,'' Instr Course Lect, **51**, pp. 315–324.

[21] Besier, T. F., Lloyd, D. G., Ackland, T. R., and Cochrane, J. L., 2001, ''Anticipatory Effects on Knee Joint Loading During Running and Cutting Maneuvers,'' Med. Sci. Sports Exercise, **33**(7), pp. 1176–1181.

[22] Besier, T. F., Lloyd, D. G., and Ackland, T. R., 2003, ''Muscle Activation Strategies at the Knee During Running and Cutting Maneuvers,'' Med. Sci. Sports Exercise, **35**(1), pp. 119–127.

[23] King, A. I., 1993, ''Progress of Research on Impact Biomechanics,'' J. Biomech. Eng., **115**(4B), pp. 582–587.

[24] Neptune, R. R., Wright, I. C., and van den Bogert, A. J., 2000, ''A Method for Numerical Simulation of Single Limb Ground Contact Events: Application to Heel-Toe Running,'' Comput. Methods Biomech. Biomed. Eng., **3**(4), pp. 321–334.

[25] Neptune, R. R., Wright, I. C., and van den Bogert, A. J., 2000, ''The Influence of Orthotic Devices and Vastus Medialis Strength and Timing on Patellofemoral Loads During Running,'' Clin. Biomech. (Los Angel. Calif.), **15**(8), pp. 611–618.

[26] Wright, I. C., Neptune, R. R., van den Bogert, A. J., and Nigg, B. M., 2000, ''The Influence of Foot Positioning on Ankle Sprains,'' J. Biomech., **33**(5), pp. 513–519.

[27] Squires, G. L., 1968, ''Practical Physics,'' McGraw Hill, London.

[28] Lu, T. W., and O'Connor, J. J., 1999, ''Bone Position Estimation From Skin Marker Co-Ordinates Using Global Optimization With Joint Constraints,'' J. Biomech., **32**(2), pp. 129–134.

[29] Yeadon, M. R., 1990, ''The Simulation of Aerial Movement—I. The Determination of Orientation Angles From Film Data,'' J. Biomech., **23**(1), pp. 59–66.

[30] Bell, A. L., Pedersen, D. R., and Brand, R. A., 1990, ''A Comparison of the Accuracy of Several Hip Center Location Prediction Methods,'' J. Biomech., **23**(6), pp. 617–621.

[31] Vaughan, C. L., Davis, B. L., and O'Connor, J. C., 1992, ''Dynamics of Human Gait,'' Human Kinetics Publishers, Champaign, IL, p. 26.

[32] Isman, R. E., and Inman, V. T., 1969, ''Anthropometric Studies of the Human Foot an Ankle,'' Bull. Prosthet. Res., **11**, pp. 97–129.

[33] van den Bogert, A. J., Smith, G. D., and Nigg, B. M., 1994, ''In Vivo Determination of the Anatomical Axes of the Ankle Joint Complex: An Optimization Approach,'' J. Biomech., **27**(12), pp. 1477–1488.

[34] de Leva, P., 1996, ''Adjustments to Zatsiorsky-Seluyanov's Segment Inertia Parameters,'' J. Biomech., **29**(9), pp. 1223–1230.

[35] Wakeling, J. M., and Nigg, B. M., 2001, ''Soft-Tissue Vibrations in the Quadriceps Measured With Skin Mounted Transducers,'' J. Biomech., **34**(4), pp. 539–543.

[36] Arnold, A. S., Salinas, S., Asakawa, D. J., and Delp, S. L., 2000, ''Accuracy of Muscle Moment Arms Estimated From MRI-Based Musculoskeletal Models of the Lower Extremity,'' Comput. Aided Surg., **5**(2), pp. 108–119.

[37] Arnold, A. S., and Delp, S. L., 2001, ''Rotational Moment Arms of the Medial Hamstrings and Adductors Vary With Femoral Geometry and Limb Position: Implications for the Treatment of Internally Rotated Gait,'' J. Biomech., **34**(4), pp. 437–447.

[38] Herzog, W., and Read, L. J., 1993, ''Lines of Action and Moment Arms of the Major Force-Carrying Structures Crossing the Human Knee Joint,'' J. Am. Aud Soc., **182**(Pt 2), pp. 213–230.

[39] Kellis, E., and Baltzopoulos, V., 1999, ''In Vivo Determination of the Patella Tendon and Hamstrings Moment Arms in Adult Males Using Videofluoroscopy During Submaximal Knee Extension and Flexion,'' Clin. Biomech. (Los Angel. Calif.), **14**(2), pp. 118–124.

[40] Klein, P., Mattys, S., and Rooze, M., 1996, ''Moment Arm Length Variations of Selected Muscles Acting on Talocrural and Subtalar Joints During Movement: An in Vitro Study,'' J. Biomech., **29**(1), pp. 21–30.

[41] Lu, T. W., and O'Connor, J. J., 1996, ''Lines of Action and Moment Arms of the Major Force-Bearing Structures Crossing the Human Knee Joint: Comparison Between Theory and Experiment,'' J. Anat., **189**(3), pp. 575–585.

[42] Nemeth, G., and Ohlsen, H., 1985, ''In Vivo Moment Arm Lengths for Hip

Extensor Muscles at Different Angles of Hip Flexion,'' J. Biomech., **18**(2), pp. 129–140.
[43] Nemeth, G., and Ohlsen, H., 1989, ''Moment Arms of Hip Abductor and Adductor Muscles Measured in Vivo by Computed Tomography,'' Clin. Biomech. (Los Angel. Calif.), **4**, pp. 133–136.
[44] Spoor, C. W., van Leeuwen, J. L., Meskers, C. G., Titulaer, A. F., and Huson, A., 1990, ''Estimation of Instantaneous Moment Arms of Lower-Leg Muscles,'' J. Biomech., **23**(12), pp. 1247–1259.
[45] van Soest, A. J., and Bobbert, M. F., 1993, ''The Contribution of Muscle Properties in the Control of Explosive Movements,'' Biol. Cybern., **69**(3), pp. 195–204.
[46] Delp, S. L., Loan, J. P., Hoy, M. G., Zajac, F. E., Topp, E. L., and Rosen, J. M., 1990, ''An Interactive Graphics-Based Model of the Lower Extremity to Study Orthopaedic Surgical Procedures,'' IEEE Trans. Biomed. Eng., **37**(8), pp. 757–767.
[47] Walker, S. M., and Schrodt, G. R., 1973, ''Segment Lengths and Thin Filament Periods in Skeletal Muscle Fibres of the Rhesus Monkey and the Human,'' Anat. Rec., **178**, pp. 63–82.
[48] Gerritsen, K. G., van den Bogert, A. J., Hulliger, M., and Zernicke, R. F., 1998, ''Intrinsic Muscle Properties Facilitate Locomotor Control—a Computer Simulation Study,'' Motor Control, **2**(3), pp. 206–220.
[49] Visser, J. J., Hoogkamer, J. E., Bobbert, M. F., and Huijing, P. A., 1990, ''Length and Moment Arm of Human Leg Muscles as a Function of Knee and Hip-Joint Angles,'' Physiol. Occup. Physiol. , **61**(5–6), pp. 453–460.
[50] Kulig, K., Andrews, J. G., and Hay, J. G., 1984, ''Human Strength Curves,'' Exerc Sport Sci. Rev., **12**, pp. 417–466.
[51] Sale, D., Quinlan, J., Marsh, E., McComas, A. J., and Belanger, A. Y., 1982, ''Influence of Joint Position on Ankle Plantarflexion in Humans,'' J. Appl. Physiol., **52**(6), pp. 1636–1642.
[52] Marsh, E., Sale, D., McComas, A. J., and Quinlan, J., 1981, ''Influence of Joint Position on Ankle Dorsiflexion in Humans,'' J. Appl. Physiol., **51**(1), pp. 160–167.
[53] He, J., Levine, W. S., and Loeb, G. E., 1991, ''Feedback Gains for Correcting Small Perturbations to Standing Posture,'' IEEE Trans. Autom. Control, **36**, pp. 322–332.
[54] Winters, J. M., and Stark, L., 1987, ''Muscle Models: What is Gained and What is Lost by Varying Model Complexity,'' Biol. Cybern., **55**(6), pp. 403–420.
[55] Aerts, P., and De Clercq, D., 1993, ''Deformation Characteristics of the Heel Region of the Shod Foot During a Simulated Heel Strike: The Effect of Varying Midsole Hardness,'' J. Sports Sci., **11**(5), pp. 449–461.
[56] Goffe, W. L., Ferrier, G. D., and Rogers, J., 1994, ''Global Optimization of Statistical Functions With Simulated Annealing,'' J. Econometrics, **60**, pp. 65–99.
[57] McLean, S. G., 2001, ''Quantification of in vivo Anterior Cruciate Ligament Elongation During Sidestep Cutting and Running—Implications for Non-Contact Ligament Injury,'' Unpublished doctoral thesis.
[58] Reinschmidt, C., van den Bogert, A. J., Nigg, B. M., Lundberg, A., and Murphy, N., 1997, ''Effect of Skin Movement on the Analysis of Skeletal Knee Joint Motion During Running,'' J. Biomech., **30**(7), pp. 729–732.
[59] Spoor, C. W., and van Leeuwen, J. L., 1992, ''Knee Muscle Moment Arms From MRI and From Tendon Travel,'' J. Biomech., **25**(2), pp. 201–206.
[60] Pandy, M. G., and Shelburne, K. B., 1997, ''Dependence of Cruciate-Ligament Loading on Muscle Forces and External Load,'' J. Biomech., **30**(10), pp. 1015–1024.
[61] Shelburne, K. B., and Pandy, M. G., 1997, ''A Musculoskeletal Model of the Knee for Evaluating Ligament Forces During Isometric Contractions,'' J. Biomech., **30**(2), pp. 163–176.
[62] Gerritsen, K. G., Nachbauer, W., and van den Bogert, A. J., 1996, ''Computer Simulation of Landing Movement in Downhill Skiing: Anterior Cruciate Ligament Injuries,'' J. Biomech., **29**(7), pp. 845–854.
[63] Woo, S. L., Hollis, J. M., Adams, D. J., Lyon, R. M., and Takai, S., 1991, ''Tensile Properties of the Human Femur-Anterior Cruciate Ligament-Tibia Complex. The Effects of Specimen Age and Orientation,'' Am. J. Sports Med., **19**(3), pp. 217–225.
[64] Besier, T. F., Lloyd, D. G., Cochrane, J. L., and Ackland, T. R., 2001, ''External Loading of the Knee Joint During Running and Cutting Maneuvers,'' Med. Sci. Sports Exercise, **33**(7), pp. 1168–1175.
[65] Piziali, R. L., Rastegar, J., Nagel, D. A., and Schurman, D. J., 1980, ''The Contribution of the Cruciate Ligaments to the Load-Displacement Characteristics of the Human Knee Joint,'' J. Biomech. Eng., **102**(4), pp. 277–283.
[66] Edman, K. A. P., 1979, ''The Velocity of Unloaded Shortening and its Relation to Sarcomere Length and Isometric Force in Vertebrate Muscle Fibers,'' J. Physiol. (London), **291**, pp. 143–159.
[67] Petrofsky, J. S., and Phillips, C. A., 1981, ''The Influence of Temperature Initial Length and Electrical Activity on the Force-Velocity Relationship of the Medial Gastrocnemius Muscle of the Cat,'' J. Biomech., **14**, pp. 297–306.
[68] Hill, A. V., 1938, ''The Heat of Shortening and the Dynamic Constants of Muscle,'' Proc. Royal Soc., **126B**, pp. 136–195.
[69] Herzog W., 1999, ''Muscle. In: Biomechanics of the Musculoskeletal System,'' 2nd Edition, edited by Nigg, B. M., and Herzog, W., Wiley, New York, pp. 148–188.
[70] Chow, J. W., and Darling, W. G., 1999, ''The Maximum Shortening Velocity of Muscle Should be Scaled With Activation,'' J. Appl. Physiol., **86**, pp. 1025–1031.
[71] Katz, B., 1939, ''The Relation Between Force and Speed in Muscular Contraction,'' J. Physiol. (London), **96**, pp. 45–64.
[72] Magnusson, S. P., Aagaard, P., Dyhre-Poulsen, P., and Kjaer, M., 2001, ''Load-Displacement Properties of the Human Triceps Surae Aponeurosis in Vivo,'' J. Physiol. (London), **531**, pp. 277–288.